European Journal of Cell Biology 102 (2023) 151357

Contents lists available at ScienceDirect

European Journal of Cell Biology

journal homepage: www.elsevier.com/locate/ejcb

Loss of the actin regulator cyclase-associated protein 1 (CAP1) modestly affects dendritic spine remodeling during synaptic plasticity

Anika Heinze [a,b], Marco B. Rust [a,b,*]

[a] Molecular Neurobiology Group, Institute of Physiological Chemistry, Philipps-University of Marburg, 35032 Marburg, Germany
[b] Center for Mind, Brain and Behavior (CMBB), University of Marburg and Justus-Liebig-University Giessen, 35032 Marburg, Germany

ARTICLE INFO

Keywords:
LTP
LTD
Long-term potentiation
Long-term depression
F-actin

ABSTRACT

Dendritic spines form the postsynaptic compartment of most excitatory synapses in the vertebrate brain. Morphological changes of dendritic spines contribute to major forms of synaptic plasticity such as long-term potentiation (LTP) or depression (LTD). Synaptic plasticity underlies learning and memory, and defects in synaptic plasticity contribute to the pathogeneses of human brain disorders. Hence, deciphering the molecules that drive spine remodeling during synaptic plasticity is critical for understanding the neuronal basis of physiological and pathological brain function. Since actin filaments (F-actin) define dendritic spine morphology, actin-binding proteins (ABP) that accelerate dis-/assembly of F-actin moved into the focus as critical regulators of synaptic plasticity. We recently identified cyclase-associated protein 1 (CAP1) as a novel actin regulator in neurons that cooperates with cofilin1, an ABP relevant for synaptic plasticity. We therefore hypothesized a crucial role for CAP1 in structural synaptic plasticity. By exploiting mouse hippocampal neurons, we tested this hypothesis in the present study. We found that induction of both forms of synaptic plasticity oppositely altered concentration of exogenous, myc-tagged CAP1 in dendritic spines, with chemical LTP (cLTP) decreasing and chemical LTD (cLTD) increasing it. cLTP induced spine enlargement in CAP1-deficient neurons. However, it did not increase the density of large spines, different from control neurons. cLTD induced spine retraction and spine size reduction in control neurons, but not in CAP1-KO neurons. Together, we report that postsynaptic myc-CAP1 concentration oppositely changed during cLTP and cTLD and that CAP1 inactivation modestly affected structural plasticity.

1. Introduction

In the vertebrate brain, most excitatory synapses are formed on small dendritic protrusions termed dendritic spines. Dendritic spines are dynamic structures that can change their size, shape or number in response to neuronal activity (Bosch and Hayashi, 2012; Yang and Liu, 2022). These morphological changes affect the function of synapses and are crucial for major forms of synaptic plasticity such as long-term potentiation (LTP) or long-term depression (LTD). Synaptic plasticity underlies brain functions like learning and memory (Citri and Malenka, 2008; Kandel et al., 2014), and defects in synaptic plasticity contribute to the pathogeneses of neuropsychiatric or neurodegenerative diseases (Shankar et al., 2008; Bourgeron, 2015; Spence and Soderling, 2015; Pelucchi et al., 2020a). Hence, elucidating the molecular mechanisms underlying structural changes during synaptic plasticity is critical for understanding the neuronal basis of physiological and pathological brain function.

Actin filaments (F-actin) form the major structural backbone of dendritic spines and thereby define spine size and shape (Bosch and Hayashi, 2012; Yang and Liu, 2022). Spine remodeling during synaptic plasticity (structural plasticity) is based on reorganization of the postsynaptic actin cytoskeleton, which requires the coordinated activity of

Abbreviations: ABP, actin-binding protein; ADF, actin depolymerizing factor; AIP1, actin interacting protein 1; AP5, (2 R)-2-Amino-5-phosphonopentanoic acid; Arp2/3, actin-related protein 2/3; ATP, adenosine triphosphate; CAP1, cyclase-associated protein 1; CAP2, cyclase-associated protein 2; cLTD, chemically induced long-term depression; cLTP, chemically induced long-term potentiation; CS, carrier solution; CTR, control; DHPG, (S)-3,5-Dihydroxyphenylglycine; DIV, days in vitro; E, embryonic day; F-actin, filamentous actin; flx, 'floxed' (flanked by loxP sites); G-actin, globular actin; GFP, green fluorescent protein; HBSS, Hanks' Balanced Salt solution; KO, knock out; LTD, long-term depression; LTP, long-term potentiation; mGluR, metabotropic glutamate receptor; PBS, phosphate-buffered saline; PFA, paraformaldehyde; pre-ind., pre-induction; PSD, postsynaptic density; RT, room temperature; STED, Stimulated Emission Depletion.

* Correspondence to: Institute of Physiological Chemistry, Philipps-University of Marburg, 35032 Marburg, Germany.
E-mail address: marco.rust@staff.uni-marburg.de (M.B. Rust).

https://doi.org/10.1016/j.ejcb.2023.151357
Received 16 May 2023; Received in revised form 22 August 2023; Accepted 24 August 2023
Available online 24 August 2023

actin-binding proteins (ABP). To date, a variety of ABP with different biochemical activities have been implicated in structural plasticity (for review: Bosch and Hayashi, 2012, Borovac et al., 2018, Okabe, 2020). Among these proteins, members of the actin depolymerizing factor (ADF)/cofilin protein family emerged as key actin regulators in dendritic spines that are relevant for synaptic plasticity (Zhou et al., 2004; Hotulainen et al., 2009; Rust et al., 2010; Gu et al., 2010; Bosch et al., 2014; Wolf et al., 2015; Rust, 2015a). Consequently, inactivation of ADF/cofilin impaired brain function and caused behavioral deficits in mice (Rust et al., 2010; Goodson et al., 2012; Wolf et al., 2015; Zimmermann et al., 2015; Rust, 2015b; Rust and Maritzen, 2015c; Sungur et al., 2018). Further, dysregulation of cofilin1, the dominant ADF/cofilin family member in the brain (Rust, 2015a), has been implicated in the pathogeneses of autism spectrum disorders, schizophrenia or Alzheimer's disease (Duffney et al., 2015; Zhang et al., 2019; Feuge et al., 2019; Pelucchi et al., 2020b; Bamburg et al., 2021).

Cyclase-associated proteins (CAP) are a family of evolutionary conserved proteins that have been implicated in actin dynamics just recently (for review: Rust et al., 2020). Specifically, these proteins cooperate with ADF/cofilin in accelerating actin subunit dissociation at filaments' minus ends, and they catalyze nucleotide exchange on globular actin monomers (G-actin) to replenish the pool of polymerization competent ATP-G-actin (Jansen et al., 2014; Kotila et al., 2018; Kotila et al., 2019; Shekhar et al., 2019). We recently reported important neuronal functions for the family member CAP1 (Schneider et al., 2021a; Schneider et al., 2021b; Heinze et al., 2022), and we identified CAP1 as a novel postsynaptic actin regulator that controls dendritic spine morphology in cooperation with cofilin1 (Heinze et al., 2022). Based on these findings and the established function of cofilin1 in synaptic plasticity we hypothesized a role for CAP1 in structural plasticity.

To test this hypothesis, we determined concentration of myc-tagged CAP1 in dendritic spines as well as spine morphology changes in CAP1-deficient hippocampal neurons upon chemical induction of structural plasticity. We found that induction of chemical LTP (cLTP) and LTD (cLTD) oppositely altered myc-CAP1 concentration in dendritic spines, with cLTP decreasing and cLTD increasing it. cLTP induced spine enlargement in CAP1-deficient neurons. However, it did not increase the fraction of large spines, unlike in control neurons. cLTD induced spine retraction and spine size reduction in control neurons, but failed to induce shrinkage of large spines in CAP1-KO neurons. Together, we report that myc-CAP1 concentration in dendritic spines oppositely changed during cLTP and cLTD and that loss of CAP1 modestly affected structural plasticity.

2. Material and methods

2.1. Transgenic mice

In this study, primary hippocampal neurons from conditional CAP1 ($CAP1^{flx/flx}$) mice were used. Generation of this strain has been described previously (Schneider et al., 2021a). $CAP1^{flx/flx}$ embryos were killed at embryonic day 18.5 (E18.5) by decapitation. $CAP1^{flx/flx}$ embryos were generated by crossing two to five months old males and females (both $CAP1^{flx/flx}$) in standard type II long mouse cages (Fa. Zoonlab). Pregnancy of female mice was controlled by vaginal plug next morning and by weight gain. Vaginal plug-positive females that gained weight were killed by cervical dislocation at the time fetuses were E18.5. In total, 50 embryos of 10 dams of $CAP1^{flx/flx}$ mice were used for this study.

Mice of the $CAP1^{flx/flx}$ colony were housed in same-sex groups of up to six animals in standard type II long mouse cages (Fa. Zoonlab) at the animal facility of the University of Marburg on 12-hour dark-light cycles with food and water available ad libitum. Treatment of mice was in accordance with the German law for conducting animal experiments and followed the guidelines for the care and use of laboratory animals of the U.S. National Institutes of Health. Killing of mice has been approved by internal animal welfare authorities (file reference AK-12–2020-Rust) and by Regierungspräsidium Giessen (file reference G13/2021).

2.2. Cell culture and transfection

Primary hippocampal neurons from E18.5 $CAP1^{flx/flx}$ mice were prepared as previously described (Schratt et al., 2006). Briefly, hippocampi of all embryos of one litter (both sexes) were pooled and dissociated in Neurobasal medium containing 2 % B27, 1 mM GlutaMax, 100 μg/ml streptomycin, and 100 U/ml penicillin (Gibco, Thermo Fischer). Neurons were plated at a density of 62,000/cm^2 on 0.1 mg/ml poly--L-lysine-coated coverslips in 24 well plates and kept in a humidified incubator at 37 °C with 5 % CO_2. Neurons derived from hippocampi of one litter were considered as one biological replicate.

Hippocampal neurons were transfected on DIV6 with 1 μg plasmid/well of 24 well plates using Lipofectamine 2000 reagent (Thermo Fischer) according to manufacturer's protocol. In all experiments, the same amount of each individual construct has been transfected. Empty pcDNA3.1 vector has been added to set total DNA amount to the desired quantity. To achieve CAP1 deletion (CAP1-KO), $CAP1^{flx/flx}$ neurons were transfected with catalytically active mCherry-Cre, which causes recombination of floxed alleles and thereby inactivation of CAP1 (Heinze et al., 2022). Neurons that were transfected with a mutated, catalytically inactive mCherry-Cre were used as control (CTR) neurons. For overexpression of CAP1, we used pcDNA3.1-CAP1-eGFP and pCMV-Myc-N-CAP1 vectors. CAP1-eGFP overexpression plasmid pcDNA3.1-CAP1-eGFP was purchased from GenScript. pCMV-Myc-N-CAP1 was generated by amplification of CAP1 open reading frame from pcDNA3.1-CAP1-eGFP plasmid and cloning it in frame between *Sal*I and *Not*I restriction sites. pGFP and pDsRed1–1 were used as volume markers. In all analyses, only neurons that have taken up all transfected constructs have been analyzed, which has been checked for each individual neuron by visual inspection at the microscope.

2.3. Chemical LTP (cLTP) induction in primary hippocampal neurons

cLTP was induced according to a previously described protocol (Feuge et al., 2019). Briefly, DIV20 primary hippocampal neurons were treated over night with 10 μM (2 R)-2-Amino-5-phosphonopentanoic acid (AP5), incubated on the next day in Mg^{2+}-containing 1x Hanks' Balanced Salt solution (HBSS; pre-induction solution) for 10 min at room temperature (RT) and subsequently stimulated for 10 min using 1x Mg^{2+}-free HBSS containing 200 μM glycine and 3 μM strychnine (stimulation solution). After cLTP induction, the stimulation solution was replaced by pre-induction solution and cells were incubated at RT for different amounts of time up to 60 min, then washed once with phosphate-buffered saline (PBS) and fixed for 15 min using 4 % paraformaldehyde (PFA)/sucrose in PBS. After washing five times with PBS, coverslips were mounted onto microscopy slides using AquaPoly/mount (Polysciences Inc.).

2.4. Chemical LTD (cLTD) induction in primary hippocampal neurons

cLTD was induced similar to a previous study (Shinoda et al., 2010). Briefly, conditioned medium of DIV21 hippocampal neurons was collected and replaced by neurobasal medium containing 100 μM (S)-3, 5-Dihydroxyphenylglycine (DHPG). After 10 min incubation at 37 °C, the DHPG-containing medium was replaced by the previously collected conditioned medium and cells were incubated at 37 °C for different amounts of time up to 120 min, then washed once with PBS and fixed for 15 min using a 4 % PFA solution. After washing five times with PBS, coverslips were mounted onto microscopy slides using AquaPoly/mount (Polysciences Inc.).

2.5. Immunocytochemistry

Neurons were washed once with PBS, fixed in a 4 % PFA solution for 15 min and rinsed in PBS three times. After 10 min incubation in carrier solution (CS; 0.1 % gelatin, 0.3 % Triton-X100 in PBS), neurons were incubated with primary antibodies (Rabbit-anti-GFP: 1:1000, Thermo Fisher Scientific, Cat. #G10362; mouse-anti-c-myc: 1:200, Thermo Fisher Scientific, Cat. #13–2500) in CS for 2 h. Thereafter, neurons were washed with PBS three times for 5 min and incubated with secondary antibodies (goat anti-rabbit-AlexaFluor488: 1:2000, Thermo Fisher Scientific, Cat. #A-11034; donkey anti-mouse-AlexaFluor647: 1:2000, Thermo Fisher Scientific, Cat. #A-31571) in CS for 45 min. After washing five times with PBS, coverslips were mounted onto microscopy slides using AquaPoly/mount (Polysciences Inc.).

2.6. Spine analysis

Image acquisition was performed with Leica TCS SP5 II LSM and LAS AF software using a 63x oil immersion objective. Confocal images were acquired with a resolution of 2048 × 2048 or 1024 × 1024 pixels as z-stacks of 9 optical planes with a step size of 0.49 µm and projected to a single-plane image (maximum projection). All analyses were performed with the ImageJ image processing package Fiji. Spine volume, density and morphology were analyzed as previously described (Heinze et al., 2022). Intensity profiles in confocal images were acquired with Fiji 'plot profile' tool. Lines were selected in a way that they cover two spines and interjacent dendritic shaft. Myc-CAP1 localization was analyzed with 'freehand selection' tool. The shape of the spine head was outlined using the GFP signal and intensity of the myc-CAP1 signal was measured in this area. The intensity of the adjacent dendritic shaft was measured in the same way and spine head signal was normalized to dendrite signal. In plots showing normalized CAP1 concentration (Fig. 2C, D, E and Fig. 4C, D, E), intensity values were additionally normalized to the area of the spine head.

2.7. Statistical analysis

The results of all experiments are based on three independent biological replicates (neurons derived from pooled hippocampi of one litter were considered as one biological replicate; N = 3). If not stated otherwise, n-values indicate the total number of analyzed neurons (first value) and the total number of analyzed spines per condition (second value, in parentheses). For example, 'n = 15 (≥225)' indicates that five neurons per condition and at least 15 spines per neuron were analyzed in each biological replicate (5 neurons × 15 spines x 3 biological replicates = 225). Except for Figs. 2F, 3C, 4F and 5C, single spine measurements were averaged for every neuron and statistics were performed with neuron's mean values. Statistical tests were performed as indicated in figure legends using GraphPad Prism 9. In all experiments, experimenters were blinded to the genotype during image acquisition and analysis, including the planned segregation of thin and mushroom-like spines.

3. Results

3.1. Enrichment of myc-CAP1 in dendritic spines

In a previous study (Heinze et al., 2022), by exploiting a green fluorescent protein (GFP)-tagged CAP1 construct (CAP1-GFP), we showed moderate, but significant enrichment of CAP1 in dendritic spines of primary hippocampal neurons obtained from embryonic day 18.5 (E18.5) mice and kept in vitro for 16 days (DIV16). Immunocytochemistry confirmed postsynaptic localization of endogenous CAP1, and super-resolution microscopy revealed CAP1 localization in spine heads underneath the postsynaptic density (PSD). Since we used a myc-tagged CAP1 construct (myc-CAP1) in the present study, we first tested whether its sub-cellular distribution was similar to CAP1-GFP. When co-transfected together with the volume marker *Discosoma* red fluorescent protein (dsRed), simultaneous expression of myc-CAP1 and CAP1-GFP with subsequent immunostaining against myc and GFP revealed a very similar distribution of both fusion proteins in the dendritic compartment (Fig. 1A). Different from the homogenously distributed volume marker, myc-CAP1 was slightly enriched in spine heads, very similar to CAP1-GFP (Fig. 1B). Spine head enrichment of myc-CAP1 was confirmed by quantifying the signal ratio between mushroom spine heads and the adjacent dendritic shaft in neurons transfected with myc-CAP1 and the volume marker GFP (Fig. 1C). While the spine/shaft ratio amounted to 0.817 ± 0.066 for GFP, we found a 60 % increase in this ratio for myc-CAP1 signal (Fig. 1D; of 1.316 ± 0.124; $p < 0.001$). This value was comparable to the one we reported for CAP1-GFP in our previous study (1.31 ± 0.07; Heinze et al., 2022). Hence, our myc-CAP1 construct is a valuable tool to study CAP1 concentration during synaptic plasticity.

3.2. Postsynaptic CAP1 concentration decreases during cLTP

To study postsynaptic CAP1 concentration during synaptic plasticity, we chemically induced LTP (cLTP) in DIV21 mouse hippocampal neurons by applying a previously published glycine-based protocol (Feuge et al., 2019). We transfected myc-CAP1 in DIV6 neurons together with GFP that we used as a volume marker to normalize CAP1 levels to spine size and, hence, to calculate CAP1 concentration in dendritic spines. Neurons were fixed either before or at different time points (0–60 min) after cLTP induction to acquire confocal images of dendritic shafts that we used to determine myc-CAP1 concentration in spines (Fig. 2A-B). As expected, myc-CAP1 was slightly enriched in spines of DIV21 neurons before cLTP induction (pre-induction). However, myc-CAP1 signal intensity visibly decreased during cLTP (Fig. 2B-C). Exemplarily, neurons fixed 30 min after cLTP induction only reached 74 % and neurons fixed 60 min after cLTP induction only reached 60 % of the concentration we observed in spines before cLTP induction (Fig. 2C; 30 min: 0.743 ± 0.080, $p < 0.05$; 60 min: 0.603 ± 0.081, $p < 0.001$).

Dendritic spines exhibit different shapes and sizes that affect their functional properties (Hering and Sheng, 2001). We therefore determined myc-CAP1 concentration in two different spine types separately, namely thin and mushroom-like spines, which reflect the largest spine type fractions (Heinze et al., 2022). In both spine types, CAP1 concentration decreased upon cLTP induction (Fig. 2D-E). In mushroom-like spines, CAP1 concentration continuously declined and amounted to 73 % of the pre-induction control after 10 min, 71 % after 30 min and 59 % after 60 min (Fig. 2D; 10 min: 0.731 ± 0.082, $p < 0.01$; 30 min: 0.708 ± 0.106, $p < 0.001$; 60 min: 0.594 ± 0.056, $p < 0.001$). In contrast, thin spines showed a peak in CAP1 concentration 10 min after cLTP induction, which was not significantly different from the pre-induction time point (Fig. 2E; 1.165 ± 1.153, $p = 0.999$). However, during cLTP progression it decreased and amounted to 57 % of pre-induction value after 60 min (0.567 ± 0.088, $p < 0.01$).

To further determine whether CAP1 concentration was dependent on spine size, we correlated myc-CAP1 concentration and spine size before and at different time points after cLTP induction by plotting both parameters in scatter diagrams (Fig. 2F). At the pre-induction time point, we found a positive Pearson correlation between CAP1 concentration and spine volume (black line, r_{total}=0.56, $p < 0.001$), which persisted during cLTP progression (0 min: r_{total}=0.54; 10 min: r_{total}=0.42; 30 min: r_{total}=0.62; 60 min: r_{total}=0.54; $p < 0.001$ for all time points). Again, we separated thin from mushroom-like spines, and, before cLTP induction, we found a positive correlation between CAP1 concentration and size for thin spines (turquoise line, r_t =0.59, $p < 0.001$), but not for mushroom-like spines (magenta line, r_m=0.02, $p = 0.905$). The positive correlation in thin spines persisted during cLTP with the exception of the 10 min time point (0 min: r_t =0.34, $p < 0.05$; 10 min: r_t =0.27, $p = 0.076$; 30 min: r_t =0.31, $p < 0.05$; 60 min: r_t =0.37, $p < 0.05$). Instead, at none

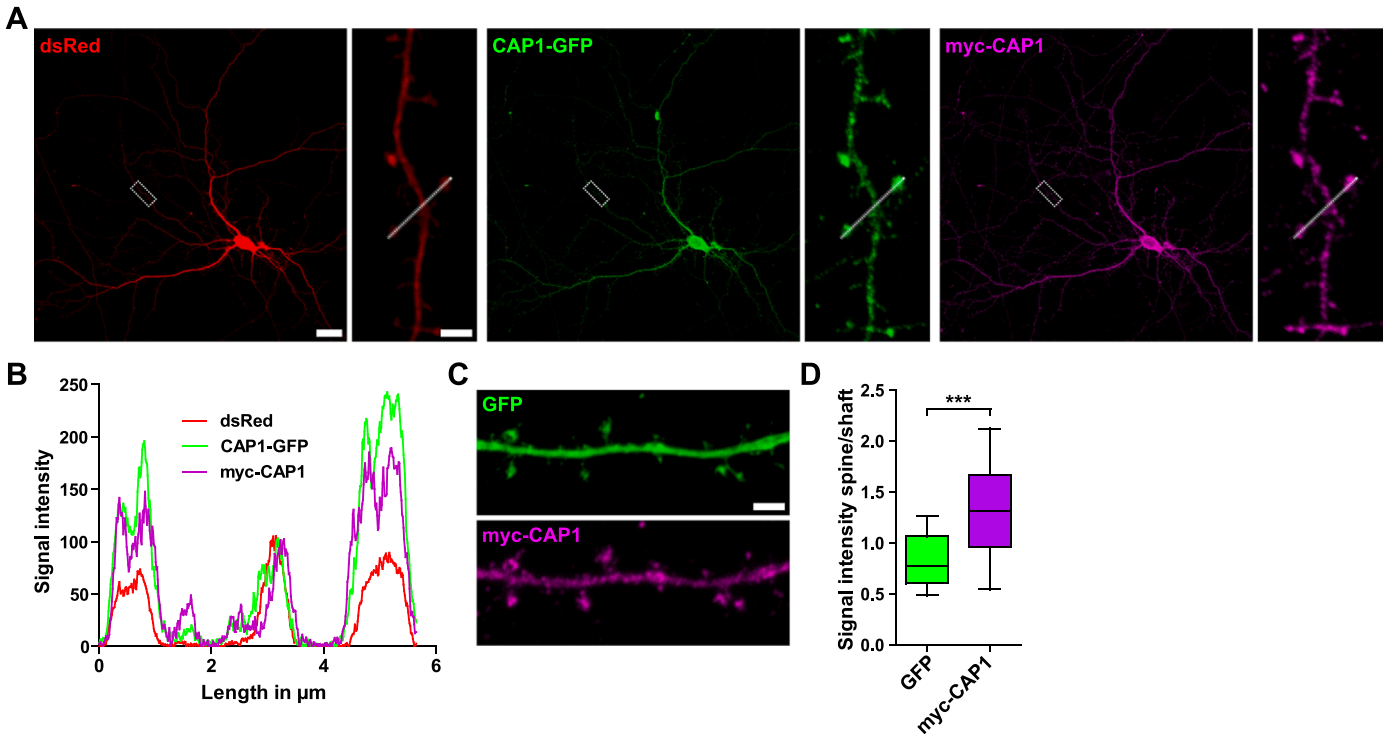

Fig. 1. Myc-CAP1 is enriched in dendritic spines. (A) Representative micrographs of DIV21 mouse hippocampal neurons expressing the volume marker dsRed (red), CAP1-GFP (green) and myc-CAP1 (magenta). Neurons were stained with antibodies against GFP and myc after fixation. Boxes indicate areas shown in higher magnification. Scale bars: 20 µm (low magnification), 2 µm (high magnification). **(B)** Fluorescence intensity profiles for dsRed, CAP1-GFP and CAP1-myc along white lines shown in A. Left-to-right direction in graph corresponds to bottom-left-to-top-right direction in micrograph. **(C)** Representative micrographs of DIV21 mouse hippocampal neurons expressing the volume marker GFP (green) and myc-CAP1 (magenta). Neurons were stained with an antibody against myc after fixation. Scale bar: 2 µm. **(D)** Signal ratio between mushroom spine heads and the adjacent dendritic shaft in neurons transfected with myc-CAP1 and the volume marker GFP. n = 15 (45), corresponding to 15 neurons per experimental group including 45 analyzed spines, N = 3, corresponding to three biological replicates. Data are represented as mean ± SEM. Paired t test was performed to test for statistical significance. ***: $p < 0.001$.

of these time point did we found a positive correlation between CAP1 concentration and size of mushroom-like spines (0 min: r_m=0.08, p = 0.602; 10 min: r_m=0.29, p = 0.052; 30 min: r_m=0.08, p = 0.587; 60 min: r_m=0.10, p = 0.521). Together, we found that CAP1 concentration was proportional to size of thin spines both before and during cLTP, but not to size of mushroom-like spines. Further, we found that CAP1 concentration decreased during cLTP progression both in thin and mushroom-like spines, especially at later time points.

3.3. CAP1 inactivation only moderately impairs cLTP-induced structural plasticity

Because substantial CAP1 levels were present in dendritic spines during and after cLTP induction, we next tested whether CAP1 was relevant for structural changes associated with cLTP. To do so, we genetically removed CAP1 from hippocampal neurons isolated from conditional CAP1 ($CAP1^{flx/flx}$) mice as previously described (Schneider et al., 2021a; Heinze et al., 2022). In our experiments, we compared cLTP-induced structural changes in DIV21 Cre-expressing $CAP1^{flx/flx}$ neurons (CAP1-KO) to $CAP1^{flx/flx}$ neurons expressing catalytically inactive Cre that served as control (CTR) neurons. While we previously reported a 27 % increase in spine volume in DIV16 CAP1-KO neurons (Heinze et al., 2022), spine enlargement was somewhat smaller in unstimulated DIV21 CAP1-KO neurons (Fig. 3B; CTR: 0.259 ± 0.015; CAP1-KO: 0.296 ± 0.018, +14 %, p = 0.398), which was likely attributable to the precedent AP5 treatment of neurons before cLTP induction (Rocha and Sur, 1995; Ouyang et al., 2005; Pinzon-Parra et al., 2022). cLTP induced an increase in spine volume in both CTR and CAP1-KO neurons (CTR 60 min: 0.333 ± 0.014, +29 %, $p < 0.01$; CAP1-KO 60 min: 0.359 ± 0.021, +21 %, $p < 0.05$). 60 min after cLTP induction, spine volume was not different between CTR and CAP1-KO neurons (p = 0.716). To better compare cLTP-induced spine enlargement, we plotted cumulative frequencies of spine volume for CTR and CAP1-KO neurons before and 60 min after cLTP induction (Fig. 3C). cLTP induced a shift towards larger spines in both CTR and CAP1-KO neurons (CTR Pre-ind. vs CTR 60 min: $p < 0.0001$; CAP1-KO Pre-ind. vs CAP1-KO 60 min: $p < 0.0001$). These curves were significantly different between CTR and CAP1-KO both before and after cLTP induction, with CAP1-KO curves being shifted to the right (CTR Pre-ind. vs CAP1-KO Pre-ind.: $p < 0.0001$; CTR 60 min vs CAP1-KO 60 min: $p < 0.01$).

The differences in cumulative frequencies of spine volumes prompted us to perform a detailed morphometric analysis and categorization of dendritic spines in CTR and CAP1-KO neurons at different time points before and after cLTP induction. Thereby, we aimed to elucidate if changes in spine type distribution or rather in the morphology of single spine types were accountable for the differences in overall spine volume. We therefore firstly determined total spine density as well as the densities of filopodia-like, thin, mushroom-like, stubby and branched spines in CTR and CAP1-KO neurons similar to previous studies (Hering and Sheng, 2001; Heinze et al., 2022). In contrast to our analysis in DIV16 neurons (Heinze et al., 2022), total spine density was not different between DIV21 CTR and CAP1-KO neurons before cLTP induction (Fig. 3D; CTR Pre-ind.: 0.963 ± 0.073 spines/µm, CAP1-KO Pre-ind.: 0.900 ± 0.042 spines/µm, p = 0.852). cLTP did not change total spine density in CTR or CAP1-KO neurons. Exemplarily, 60 min after cLTP induction, total spine density amounted to 0.978 ± 0.046 spines/µm in CTR neurons (p = 0.996 when compared to CTR Pre-ind.) and to 0.853 ± 0.045 spines/µm in CAP1-KO neurons (p = 0.886 when compared to CAP1-KO Pre-ind.). However, consistent with our previous analysis in DIV16

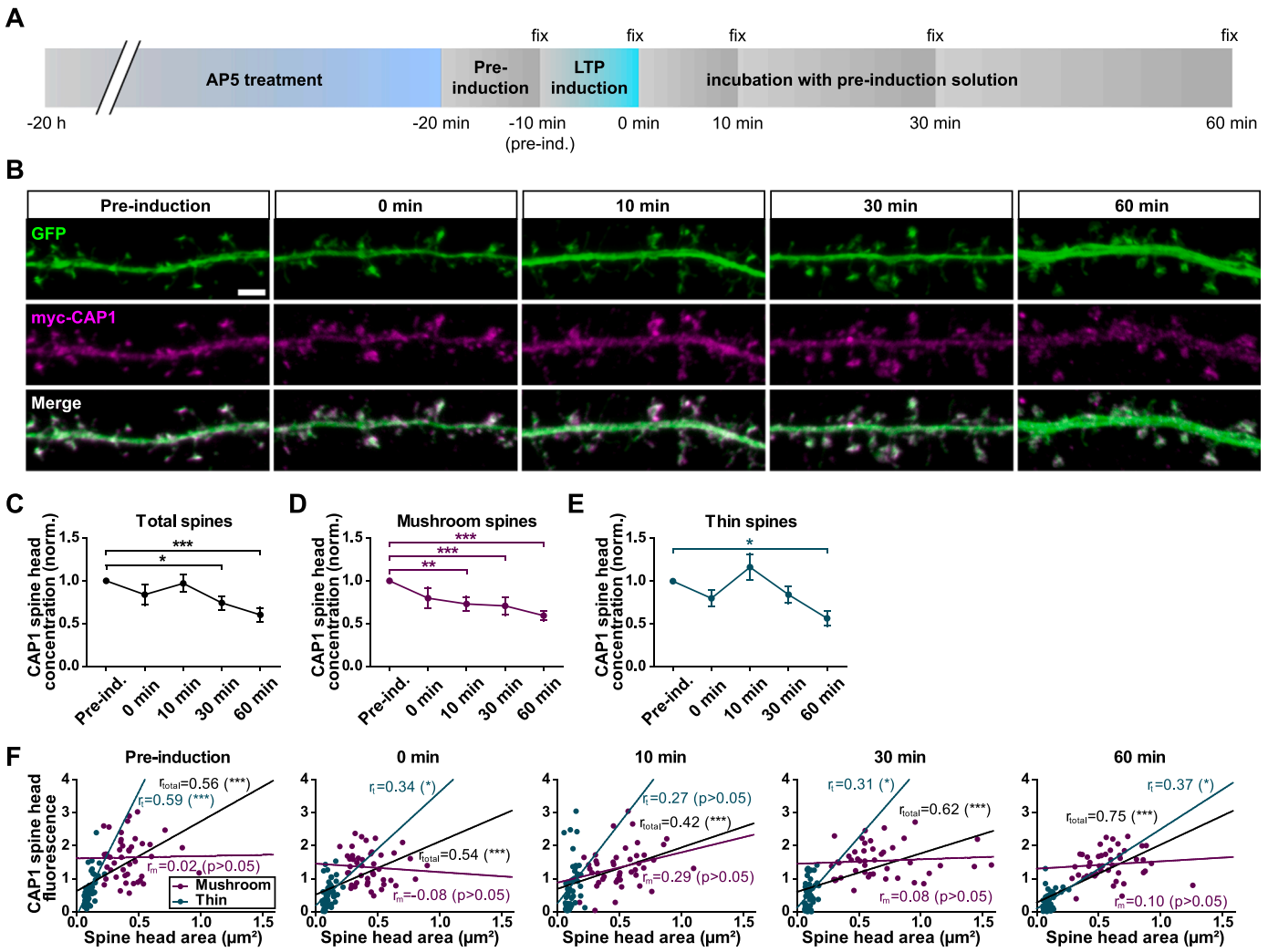

Fig. 2. Myc-CAP1 spine head concentration declines after cLTP induction. **(A)** cLTP induction protocol. Mouse primary hippocampal neurons were treated with AP5 overnight, stimulated with cLTP-inducing medium on DIV21 and fixed at indicated time points before or after cLTP induction (for detailed description, see material and methods). **(B)** cLTP was induced in neurons transfected with GFP (green) and myc-CAP1 (magenta). Representative confocal images of dendrite sections of neurons fixed either before (Pre-induction) or 0 min, 10 min, 30 min and 60 min after cLTP induction. Neurons were stained with an antibody against myc after fixation. Scale bar: 2 µm. **(C)** Spine head concentration of myc-CAP1 declines during cLTP progression. n ≥ 14 (≥84), N = 3. **(D)** Spine head concentration of myc-CAP1 in mushroom-like spines declines during cLTP progression. n ≥ 14 (≥42), N = 3. **(E)** Spine head concentration of myc-CAP1 in thin spines peaks at 10 min and declines thereafter during further cLTP progression. n ≥ 14 (≥42), N = 3. Values of the pre-induction time point in C, D, E were set as 1 and data are represented as mean ± SEM. One-way ANOVA followed by Dunnett's multiple comparison test was performed prior to normalization to the pre-induction control to test for statistical significance. Significance information shown in C, D, E represent the comparison to the respective pre-induction control. Statistical comparison to the pre-induction control was performed for all time points, but only significant comparisons ($p < 0.05$) are indicated by asterisks. **(F)** Scatter plots showing correlation of myc-CAP1 levels and spine size at different time points after cLTP induction. n = 15 (90), N = 3 for every time point. Linear correlation was tested by Pearson correlation analysis. r: Pearson correlation coefficient for total spines (r_{total}), thin spines (r_t) and mushroom spines (r_m). *: $p < 0.05$, **: $p < 0.01$, ***: $p < 0.001$.

neurons (Heinze et al., 2022), distribution of single spine types was altered in non-stimulated DIV21 CAP1-KO neurons. While there were no differences in the densities of filopodia-like, stubby, mushroom-like and branched spines, we found a significantly reduced number of thin spines in CAP1-KO neurons when compared to CTR neurons (Fig. 3E; CTR Pre-ind.: 0.366 ± 0.042 spines/µm, CAP1-KO Pre-ind.: 0.275 ± 0.026 spines/µm, −25 %, $p < 0.05$). cLTP induced a decrease in thin spines in CTR neurons (10 min: 0.279 ± 0.039 spines/µm, −24 %, $p < 0.05$ vs. Pre-ind., 30 min: 0.316 ± 0.021 spines/µm, $p = 0.584$ vs. Pre-ind., 60 min: 0.258 ± 0.023 spines/µm, −30 %, $p < 0.01$ vs. Pre-ind.), but not in CAP1-KO neurons (10 min: 0.241 ± 0.036 spines/µm, $p = 0.918$ vs. Pre-ind., 30 min: 0.356 ± 0.025 spines/µm, $p = 0.062$ vs. Pre-ind., 60 min: 0.236 ± 0.017 spines/µm, $p = 0.832$ vs. Pre-ind.). As expected, 60 min after cLTP induction, the density of mushroom-like spines was significantly increased compared to the pre-induction time point in CTR neurons (Pre-ind.: 0.381 ± 0.030 spines/µm, 60 min: 0.471 ± 0.030 spines/µm, +24 %, $p < 0.05$). In CAP1-KO neurons, however, mushroom-like spine density was not different from the pre-induction time point 60 min after cLTP induction (Pre-ind.: 0.382 ± 0.017 spines/µm, 60 min: 0.417 ± 0.030 spines/µm, $p = 0.909$). Overall, we did not observe any significant changes in the densities of all analyzed spine types upon cLTP induction in CAP1-KO neurons. 60 min after cLTP, there were no significant differences in spine type densities between CTR and CAP1-KO neurons.

Since we ruled out alterations in spine type distribution as a cause for cLTP-induced increase in spine volume in CAP1-KO neurons, we next performed detailed spine morphometric analysis to examine changes in spine morphology upon cLTP induction. We measured total spine length and head width (all spine types taken together) as well as length and head width of filopodia-like, thin, stubby and mushroom-like spines of CTR and CAP1-KO spines before and after cLTP (Fig. 3F, S1). Our analysis revealed no significant changes in total spine length during

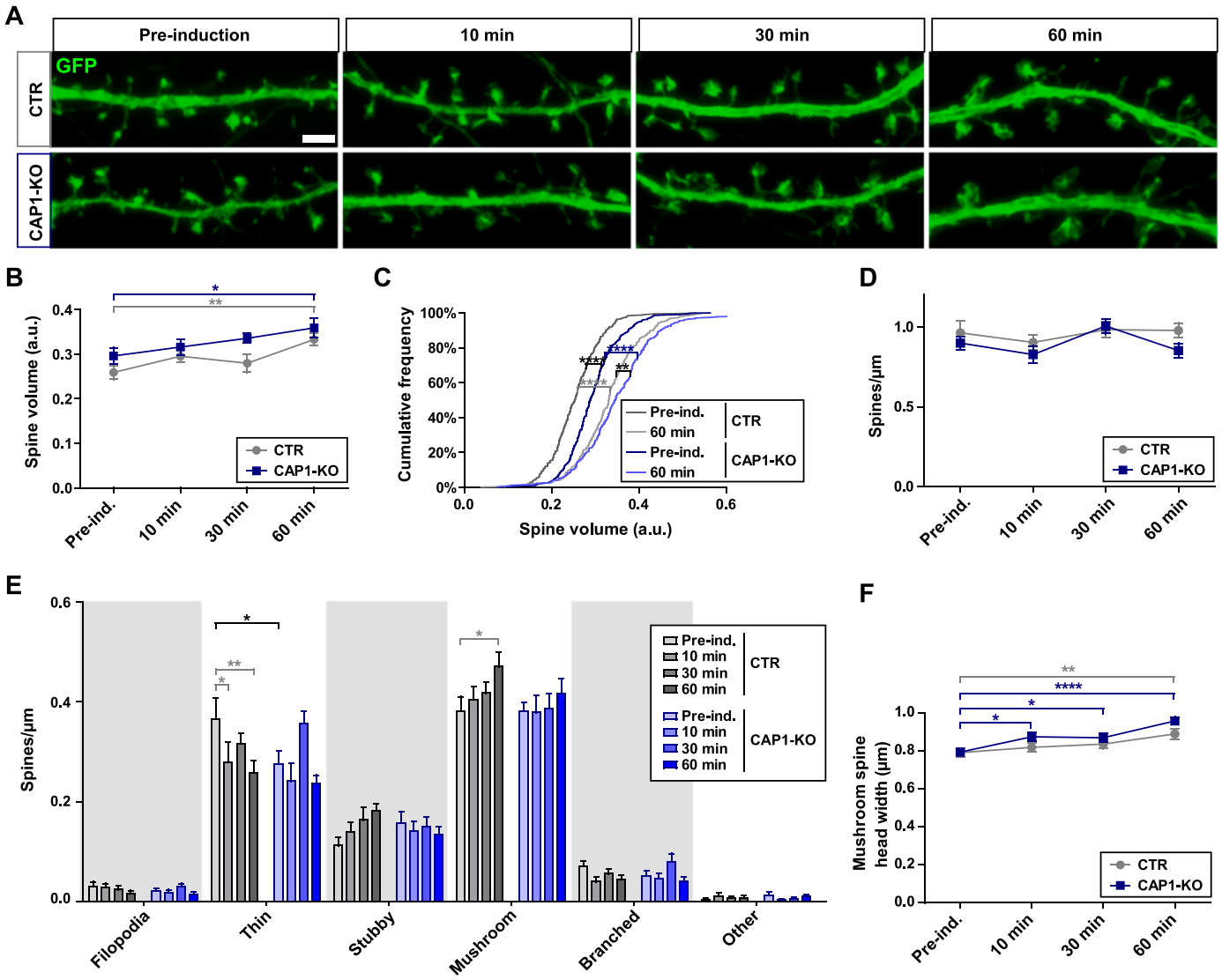

Fig. 3. Loss of CAP1 moderately affects structural changes during cLTP. (A) Representative micrographs of GFP-expressing (green) DIV21 CTR and CAP1-KO hippocampal neurons either before or after cLTP induction. Scale bar: 2 µm. **(B)** Average spine volume increases similarly in CTR and CAP1-KO neurons upon cLTP induction. Data are represented as mean ± SEM. Two-way ANOVA with Šidák's multiple comparisons test. n = 9 (≥2000), N = 3. **(C)** Cumulative curve of spine volumes in CTR and CAP1-KO neurons before and 60 min after cLTP induction. The curve is shifted towards larger spine volumes 60 min after cLTP induction in CTR and CAP1-KO neurons. Kolmogorov-Smirnov test was performed to test for statistical significance. n = 9 (≥2000), N = 3. **(D)** Total spine density does not change upon cLTP induction in CTR and CAP1-KO neurons. Data are represented as mean ± SEM. Two-way ANOVA with Šidák's multiple comparisons test. n = 15 (≥225), N = 3. **(E)** Density of thin spines decreases, and density of mushroom-like spines increases upon cLTP induction in CTR neurons. cLTP does not induce spine type density changes in CAP1-KO neurons. Data are represented as mean ± SEM. Two-way ANOVA with Tukey's multiple comparisons test. n = 15 (≥225), N = 3. **(F)** Spine head width of mushroom-like spines increases slightly faster in CAP1-KO neurons. Data are represented as mean ± SEM. Two-way ANOVA with Šidák's multiple comparisons test. n = 15 (≥225), N = 3. Significance information shown in black represent the comparison between CTR and CAP1-KO. Values shown in grey (CTR) and blue (CAP1-KO) represent the comparison to the respective pre-induction control. Statistical tests were always performed for every time point, but only significant comparisons ($p < 0.05$) are indicated by asterisks. *: $p < 0.05$, **: $p < 0.01$, ***: $p < 0.001$, ****: $p < 0.0001$.

cLTP in CTR and CAP1-KO neurons (Fig. S1A). In line with the increase in spine volume, total spine head width was elevated by 18 % in CTR and by 19 % in CAP1-KO neurons 60 min after cLTP induction when compared to pre-induction control (Fig. S1B, CTR Pre-ind.: 0.557 ± 0.018, CTR 60 min: 0.657 ± 0.020, $p < 0.01$; CAP1-KO Pre-ind.: 0.589 ± 0.014, CAP1-KO 60 min: 0.699 ± 0.016, $p < 0.001$). After 60 min, total spine head width was not significantly different between CTR and CAP1-KO neurons ($p = 0.444$). When we analyzed spine types individually, we found that head size of mushroom-like spines increased upon cLTP induction in CTR and CAP1-KO neurons (Fig. 3F). However, we observed a slightly faster and overall stronger increase in CAP1-KO neurons, which was significantly different from the pre-induction control already 10 min after cLTP induction (CAP1-KO Pre-ind.: 0.794 ± 0.015; CAP1-KO 10 min: 0.875 ± 0.022, $p < 0.05$) and amounted to 121 % of the pre-induction control after 60 min (CAP1-KO 60 min: 0.058 ± 0.020, $p < 0.0001$). This increase was not significant before 60 min in CTR neurons, where it amounted to 113 % of the pre-induction control (CTR Pre-ind.: 0.791 ± 0.022; CTR 10 min: 0.819 ± 0.023, $p = 0.761$; CTR 30 min: 0.836 ± 0.024, $p = 0.388$; CTR 60 min: 0.890 ± 0.026, $p < 0.01$). Although head width of mushroom-like spines was slightly bigger in CAP1-KO than in CTR neurons 60 min after cLTP induction, statistical comparison revealed no significant difference ($p = 0.108$).

Together, cLTP induced spine enlargement in CTR and CAP1-KO neurons, albeit cLTP-induced structural changes differed between both groups. In CTR neurons, we observed a notable cLTP-induced change in

spine type distribution towards larger spines, which was not present in CAP1-KO neurons. However, head width of mushroom-like spines increased in CAP1-KO neurons during cLTP, and this increase was somewhat stronger when compared to CTR neurons.

3.4. Postsynaptic CAP1 concentration increases during cLTD

Since cLTP-induced structural plasticity was only modestly affected in CAP1-KO neurons, we next tested whether CAP1 was more relevant for another paradigm of synaptic plasticity, namely LTD. Opposite to LTP, LTD is associated with a weakening of synaptic connections as well

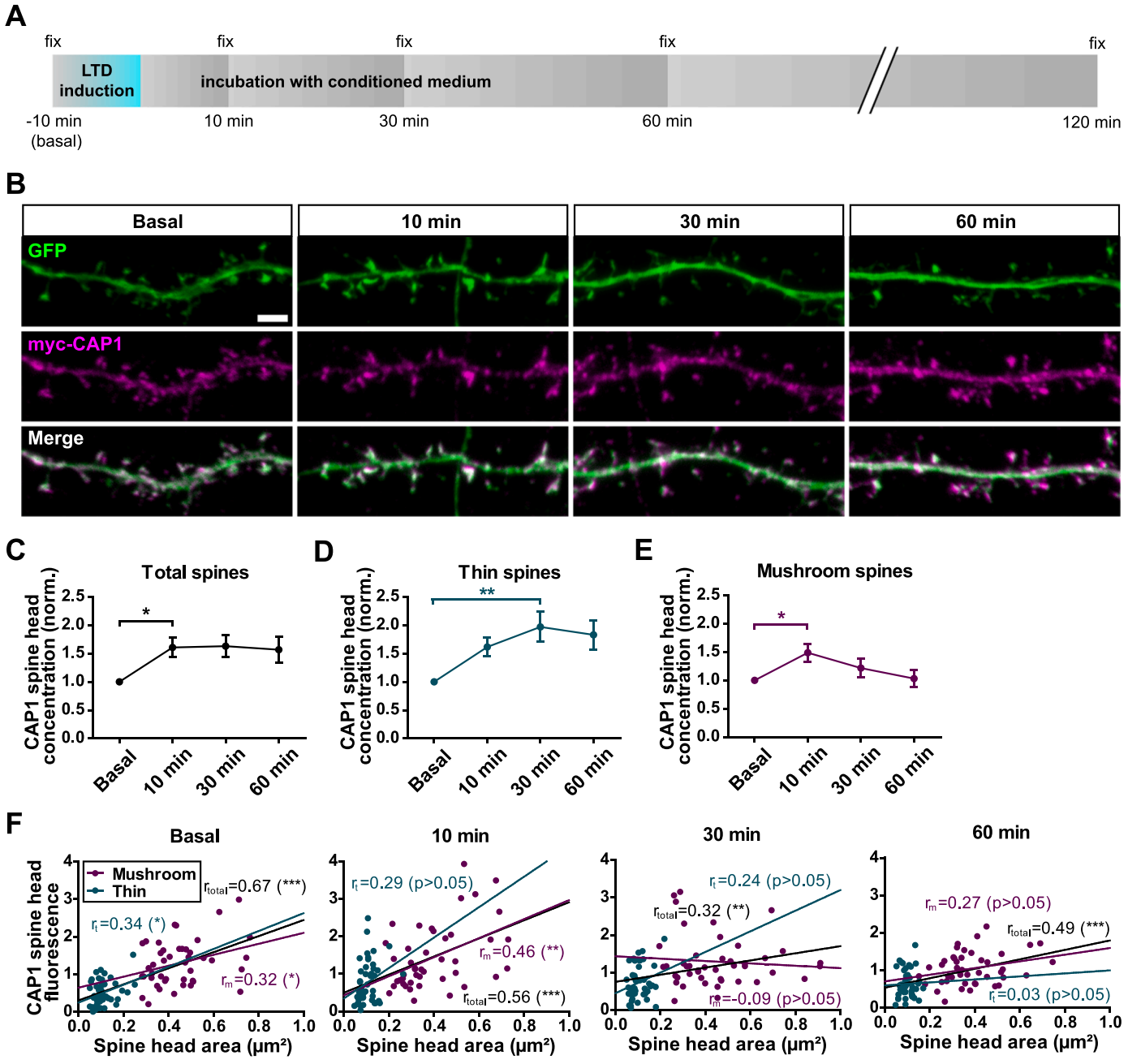

Fig. 4. Myc-CAP1 spine head concentration increases during cLTD. (A) cLTD induction protocol. Mouse primary hippocampal neurons (DIV21) were stimulated with cLTD-inducing medium and fixed at indicated time points before or after cLTD induction (for detailed description, see material and methods). **(B)** cLTD was induced in neurons transfected with GFP (green) and CAP1-myc (magenta). Representative confocal images of dendrite sections of neurons fixed either before (Basal) or 10 min, 30 min and 60 min after cLTD induction. Neurons were stained with an antibody against myc after fixation. Scale bar: 2 µm. **(C)** Spine head concentration of myc-CAP1 in spines increases during cLTD progression. n = ≥14 (≥84), N = 3. **(D)** Spine head concentration of myc-CAP1 in thin spines increases during cLTD progression. n ≥ 14 (≥42), N = 3. **(E)** Spine head concentration of myc-CAP1 in mushroom-like spines peaks at 10 min, then declines during further progression of cLTD. n ≥ 14 (≥42), N = 3. Values of the basal time point in C, D, E were set as 1 and data are represented as mean ± SEM. One-way ANOVA followed by Dunnett's multiple comparison test was performed prior to normalization to the pre-induction control to test for statistical significance. Significance information shown in C, D, E represent the comparison to the respective pre-induction control. Statistical comparison to the pre-induction control was performed for all time points, but only significant comparisons ($p < 0.05$) are indicated by asterisks. **(F)** Scatter plots showing correlation of myc-CAP1 enrichment and spine size at different time points after cLTD induction. n = 15 (90), N = 3 for every time point. Linear correlation was tested by Pearson correlation analysis. r: Pearson correlation coefficient for total spines (r_{total}), thin spines (r_t) and mushroom spines (r_m). *: $p < 0.05$, **: $p < 0.01$, ***: $p < 0.001$.

as spine shrinkage caused by F-actin disassembly (Okamoto et al., 2004; Tada and Sheng, 2006; Bosch and Hayashi, 2012). First, we tested whether chemical LTD (cLTD), induced by activation of metabotropic glutamate receptor (mGluR), changed CAP1 concentration in dendritic spines from DIV21 neurons (Fig. 4A). As for cLTP experiments, DIV6 neurons were transfected with myc-CAP1 and GFP. Before cLTD induction, myc-CAP1 was slightly enriched in spines of DIV21 hippocampal neurons (Fig. 4B), as shown for the pre-induction time point during cLTP experiments (Fig. 2B). After cLTD induction, myc-CAP1 concentration in spines increased and amounted to 160 % of control levels (before LTD) 10 min after cLTD induction (Fig. 4C; 1.607 ± 0.170, $p < 0.05$). As for cLTP experiments, we determined cLTD-induced changes in postsynaptic CAP1 concentration in thin and mushroom-like spines separately. CAP1 concentration in thin spines increased during cLTD to almost 200 % after 30 min and still amounted to 180 % of control levels 60 min after cLTD induction, although this comparison did not reach statistical significance (Fig. 4D; 30 min: 1.970 ± 0.265, $p < 0.01$; 60 min: 1.829 ± 0.262; $p = 0.161$). Instead, CAP1 concentration was increased by only 49 % in mushroom-like spines 10 min after cLTD induction, and they decreased to basal levels thereafter (Fig. 4E; 10 min: 1.490 ± 0.156, $p < 0.05$; 30 min: 1.219 ± 0.158, $p = 0.745$; 60 min: 1.032 ± 0.145, $p = 0.990$).

We next tested whether CAP1 concentration was proportional to spine size during cLTD. As for cLTP experiments, we found a strong positive Pearson correlation between both parameters before cLTD induction (black line; r_{total}=0.67, $p < 0.001$). The positive correlation persisted during cLTD progression, though the slope of the regression line flattened (10 min: r_{total}=0.56, $p < 0.001$; 30 min: r_{total}=0.32, $p < 0.01$; 60 min: r_{total}=0.49, $p < 0.001$). When analyzing thin and mushroom-like spines separately, we found a positive Pearson correlation between CAP1 concentration and spine size before cLTD induction for both spine types (thin: turquoise line, r_t =0.34, $p < 0.05$; mushroom-like: magenta line, r_m=0.32, $p < 0.05$). In mushroom-like spines, this correlation transiently increased 10 min after cLTD induction and declined thereafter (10 min: r_m=0.46, $p < 0.01$; 30 min: r_m=−0.09, $p = 0.582$; 60 min: r_m=0.27, $p = 0.074$). Instead, we noted no positive correlation in thin spines during cLTD progression (10 min: r_t =0.29, $p = 0.055$; 30 min: r_t =0.24, $p = 0.118$; 60 min: r_t =0.03, $p = 0.831$). Together, our data revealed increasing postsynaptic CAP1 concentration during cLTD induction. This increase was stronger in thin spines when compared to mushroom-like spines, and it only persisted in thin spines during cLTD progression.

3.5. Structural plasticity during cLTD is impaired in CAP1-KO-deficient neurons

Increased postsynaptic CAP1 concentration during cLTD forced us to test whether CAP1 was relevant for cLTD-induced structural plasticity. To do so, we applied the above-mentioned cLTD protocol in CTR and CAP1-KO neurons (Fig. 5A). First, we determined average spine volume during cLTD progression and found a slight, yet not significant, decrease in CTR neurons (Fig. 5B, basal: 0.198 ± 0.009; 30 min: 0.175 ± 0.010, $p = 0.418$; 60 min: 0.172 ± 0.010, $p = 0.321$; 120 min: 0.183 ± 0.013, $p = 0.741$). Surprisingly, spine volume tended to increase in CAP1-KO neurons (basal: 0.211 ± 0.016; 30 min: 0.220 ± 0.006, $p = 0.944$; 60 min: 0.229 ± 0.014, $p = 0.632$; 120 min: 0.225 ± 0.013, $p = 0.783$). While neither the decrease in average spine volume in CTR cells nor the increase in spine volume of CAP1-KO was significant within the experimental group, spine volume was significantly different between CTR and CAP1-KO at 30 min ($p < 0.05$) and 60 min ($p < 0.01$) time points. We investigated the changes in spine volume in more detail and found that cLTD caused different changes in the cumulative curves for spine volume in CTR and CAP1-KO neurons (Fig. 5C). As expected, the cumulative curve shifted to the left, towards smaller spines in CTR neurons ($p < 0.0001$). Instead, cLTD induced a right shift towards larger spines in CAP1-KO neurons ($p < 0.0001$).

As for cLTP experiments, we next determined total spine density as well as the densities of spine types before and during cLTD in CTR and CAP1-KO neurons (Fig. 5D). 30 min after cLTD induction, total spine density was reduced by roughly 30 % in CTR neurons when compared to basal levels (basal: 1.362 ± 0.117 spines/μm, 30 min: 0.938 ± 0.057 spines/μm, $p < 0.01$). Total spine density in CTR neurons was also lower at later time points, but these reductions did not reach significance (60 min: 1.173 ± 0.096 spines/μm, −14 %, $p = 0.341$; 120 min: 1.078 ± 0.067 spines/μm, −21 %, $p = 0.073$). When compared to CTR neurons, total spine density was reduced by 25 % in CAP1-KO neurons before cLTD induction (1.032 ± 0.058 spines/μm, $p < 0.05$), in line with our previous study (Heinze et al., 2022). During cLTD, total spine density in CAP1-KO neurons further decreased, but these changes did not reach significance when compared to basal levels (30 min: 0.940 ± 0.086 spines/μm, −9 %, $p = 0.841$; 60 min: 0.915 ± 0.113 spines/μm, −12 %, $p = 0.721$; 120 min: 0.816 ± 0.082 spines/μm, −21 %, $p = 0.233$). When determining spine type densities, we found that cLTD induced a reduction in both of the most prominent spine types, namely thin and mushroom-like spines, in CTR neurons (Fig. 5E). While thin spines amounted to 0.605 ± 0.093 spines/μm in the basal condition, they were reduced by 28 % 30 min after cLTD induction (30 min: 0.435 ± 0.027, $p < 0.05$). 60 and 120 min after cLTD induction, thin spine density was still lower than the basal level, but these comparisons did not reach statistical significance (60 min: 0.499 ± 0.071, $p = 0.418$, 120 min: 0.482 ± 0.087, $p = 0.229$). Density of mushroom-like spines was reduced by 37 % 30 min after cLTD induction in CTR neurons (basal: 0.438 ± 0.043, 30 min: 0.274 ± 0.035, $p < 0.05$). As for thin spines, density of mushroom-like spines was still smaller 60 and 120 min after cLTD induction, but these comparisons did not reach statistical significance (60 min: 0.361 ± 0.052, $p = 0.787$, 120 min: 0.285 ± 0.038, $p = 0.050$). Similar to our previous experiments (Heinze et al., 2022), thin spine density in CAP1-KO neurons was reduced by 32 % compared to CTR neurons before cLTD induction (CAP1-KO Basal: 0.409 ± 0.047, $p < 0.01$). Thin spine density tended to further decrease after cLTD induction in CAP1-KO neurons, yet these changes were not statistically significant compared to CAP1-KO basal level (30 min: 0.323 ± 0.028, $p = 0.684$, 60 min: 0.346 ± 0.077, $p = 0.917$, 120 min: 0.278 ± 0.059, $p = 0.160$). When compared to CTR neurons, however, thin spine density was reduced by 42 % ($p < 0.01$) after 120 min in CAP1-KO neurons. Density of mushroom-like spines did not change in CAP1-KO neurons upon cLTD induction (basal: 0.362 ± 0.036, 30 min: 0.306 ± 0.054, $p = 0.954$ vs. basal, 60 min: 0.390 ± 0.041, $p = 0.999$ vs. basal, 120 min: 0.343 ± 0.029, $p = 0.999$ vs. basal).

When we analyzed different morphological spine parameters (Fig. S2), we found that the length of spines was significantly increased in CAP1-KO neurons 30 min after cLTD induction, whereas we did not observe any changes in spine length in CTR neurons (CTR basal: 1.269 ± 0.115, CTR 30 min; 1.462 ± 1.109, $p = 0.411$; CAP1-KO basal: 1.430 ± 0.089, CAP1-KO 30 min: 1.768 ± 0.129, $p < 0.05$). Total spine head width did not significantly change in CTR and CAP1-KO neurons, however, we observed a slight upwards trend in CAP1-KO neurons. Further, analyzing morphology of individual spine types during cLTD did not reveal any gross changes (Fig. S2). When compared to basal levels, solely lengths of thin and mushroom-like spines were increased at 30 min time point in CAP1-KO neuron (thin: basal: 1.072 ± 0.055, 30 min: 1.354 ± 0.064, $p < 0.05$; mushroom: basal: 1.561 ± 0.073, 30 min: 1.900 ± 0.117, $p < 0.05$), while all other parameters were not significantly different from basal levels in CTR and CAP1-KO neurons. Together, these results suggest that cLTD induced retraction of dendritic spines as well as an overall reduction in spine size in CTR neurons, but not in CAP1-KO neurons.

4. Discussion

In the present study, we report altered concentration of exogenously expressed myc-CAP1 in dendritic spines upon induction of synaptic

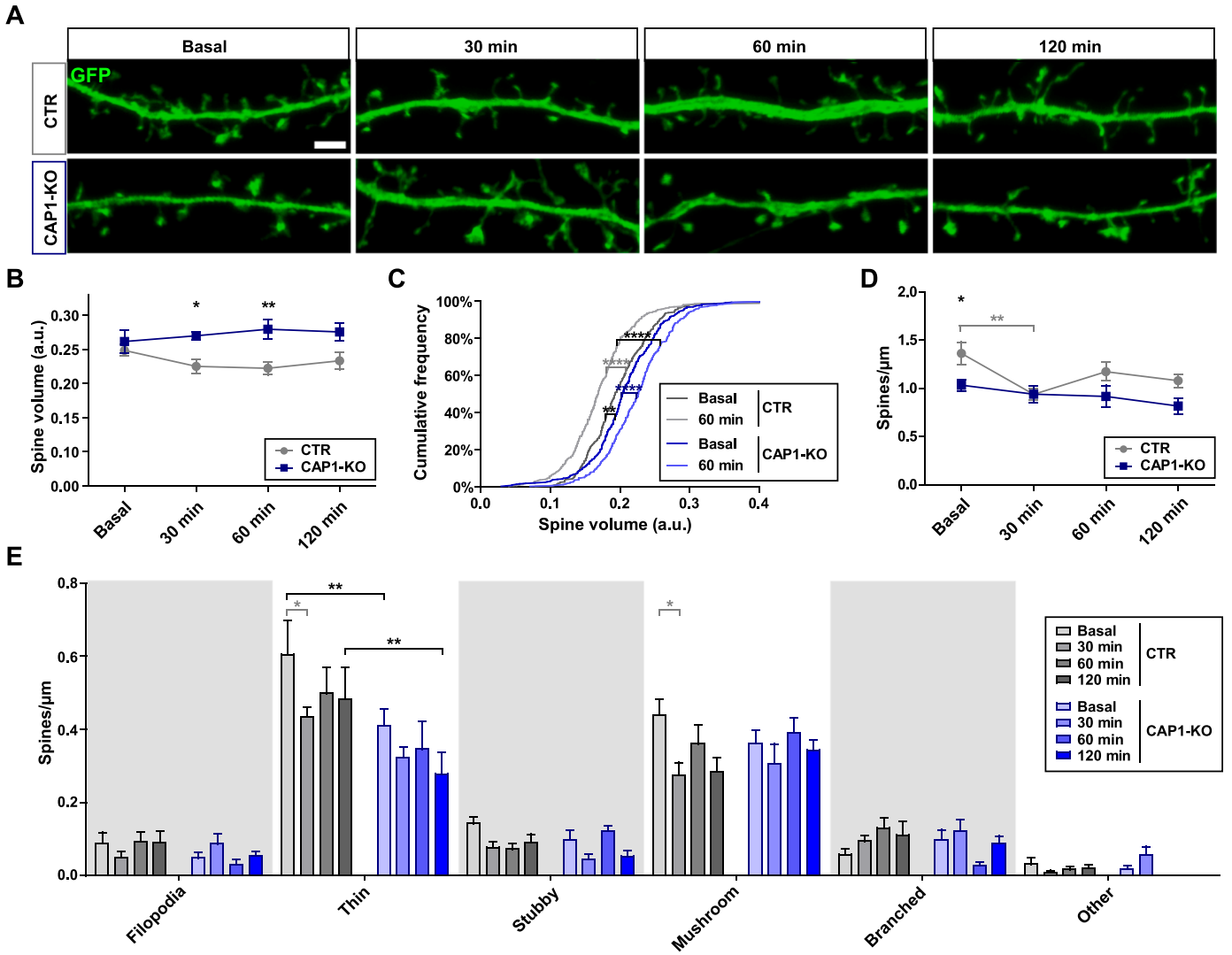

Fig. 5. Loss of CAP1 impairs structural changes during cLTD. (A) Representative micrographs of GFP-expressing (green) DIV21 CTR and CAP1-KO hippocampal neurons before and after cLTD induction. Scale bar: 2 µm. **(B)** Average spine volume in CAP1-KO neurons is different from CTR neurons 30 and 60 min after cLTD induction. Data are represented as mean ± SEM. Two-way ANOVA with Šidák's multiple comparisons test. n = 9 (≥2000), N = 3. **(C)** Cumulative frequency of spine volumes in CTR and CAP1-KO neurons before and 60 min after cLTD induction. The curve is shifted towards smaller spine volumes in CTR neurons, but towards larger spine volumes in CAP1-KO neurons. Kolmogorov-Smirnov test was performed to test for statistical significance. n = 9 (≥2000), N = 3. **(D)** Total spine density in CAP1-KO neurons is different from CTR neurons under basal conditions. Spine density significantly decreases 30 min after cLTD induction in CTR, but not in CAP1-KO neurons. Data are represented as mean ± SEM. Two-way ANOVA with Šidák's multiple comparisons test was performed to test for statistical significance in total spine density. n = 9 (≥135), N = 3. **(E)** Densities of thin and mushroom-like spines decrease after cLTD induction in CTR neurons. Only thin, but not mushroom-like spine density, is slightly reduced after cLTD in CAP1-KO neurons. Data are represented as mean ± SEM. Two-way ANOVA with Tukey's multiple comparisons test. n = 9 (≥135), N = 3. Significance information shown in black represent the comparison between CTR and CAP1-KO. Values shown in grey (CTR) and blue (CAP1-KO) represent the comparison to the respective pre-induction control. Statistical tests were always performed for every time point, but only significant comparisons ($p < 0.05$) are indicated by asterisks. *: $p < 0.05$, **: $p < 0.01$, ***: $p < 0.001$, ****: $p < 0.0001$.

plasticity: cLTP induced a decrease in postsynaptic myc-CAP1 concentration, while cLTD induction increased it. Further, we found that CAP1-deficient neurons showed some modest defects in spine remodeling associated with synaptic plasticity, especially in LTD-induced morphological changes.

In a previous study, we showed postsynaptic localization of the actin regulator CAP1 in excitatory synapses (Heinze et al., 2022). Specifically, STED microscopy revealed localization of endogenous CAP1 in spine heads, underneath the PSD. Moreover, fluorescence intensity of exogenously expressed CAP1-GFP in dendritic spines was higher when compared to GFP-expressing neurons, demonstrating a moderate, yet significant enrichment of GFP-CAP1 in dendritic spines. Similarly, we found myc-CAP1 to be slightly enriched in dendritic spines and that postsynaptic myc-CAP1 levels correlated with dendritic spine size in unstimulated neurons. Hence, postsynaptic CAP1 concentration seems to be proportional to spine size as previously reported for β-actin or various actin regulators including cofilin1, actin interacting protein 1 (AIP1), actin-related protein 2/3 (Arp2/3) complex subunits or profilin2 (Bosch et al., 2014). Our data thereby promote the notion that unstimulated dendritic spines have a similar protein composition irrespective of their size. Interestingly, a previous study reported a persistent increase in postsynaptic cofilin1 concentrations during 30 min of LTP progression, while concentrations of the other proteins returned to basal levels after an initial increase (β-actin, AIP1, Arp2/3 subunits) or an initial decrease (profilin2, Bosch et al., 2014). In contrast to β-actin and these actin regulators, we here found a persistent decrease in postsynaptic myc-CAP1 concentration during cLTP progression, which amounted to roughly 60 % of basal levels in both thin and mushroom-like spines 60 min after cLTP induction. This was highly surprising to us, because we previously reported functional interdependence of CAP1 and cofilin1 in regulating dendritic spine morphology (Heinze et al., 2022), and we therefore expected an increase in postsynaptic CAP1 concentration during cLTP as shown for cofilin1 (Bosch et al., 2014).

In line with its rapid translocation into dendritic spines upon LTP induction, cofilin1 plays a crucial role in regulating structural and functional modifications of excitatory synapses during LTP (Rust et al., 2010; Gu et al., 2010; Bosch et al., 2014). LTP is associated with an enlargement of dendritic spines, which is driven by actin polymerization and F-actin assembly (Okamoto et al., 2004; Tada and Sheng, 2006, Bosch, 2012 #2). A role for cofilin1 in LTP-induced structural plasticity therefore seems to be odd with its function as a F-actin disassembly factor. However, during the initial phase of LTP, local actin concentration increased in dendritic spines (Bosch et al., 2014). At high actin concentration, instead of F-actin depolymerization, cofilin1 may rather promote actin polymerization as cofilin1-dependent F-actin severing creates free filaments' barbed-ends that allow nucleation of new filament growth (Oser and Condeelis, 2009). Since newly formed filaments are the preferred site for branching activity of the Arp2/3 complex (Ichetovkin et al., 2002), it has been speculated that the synergistic activity of cofilin1 and Arp2/3 promotes spine enlargement during LTP (Bosch et al., 2014). This would be in line with a previous study, which suggested that during LTP larger F-actin structures are first cut into smaller filaments that quickly extend and thereby expand the actin cytoskeleton in dendritic spines (Chen et al., 2015). While early studies suggested a role for CAP1 in accelerating cofilin1-mediated F-actin severing (Normoyle and Brieher, 2012; Chaudhry et al., 2013; Jansen et al., 2014), a more recent study demonstrated that CAP1 transiently interacts with filaments pointed-ends, and that it efficiently accelerates cofilin1-mediated actin dissociation from pointed-ends, but not cofilin1-mediated F-actin severing (Kotila et al., 2019). We here report that cLTP induced spine enlargement in CAP1-KO neurons, in which the spine type distribution, however, did not shift towards larger spines. Hence, CAP1 appeared to play only a minor role in LTP-induced structural plasticity, at least during cLTP induced at room temperature. However, our findings are in line with the studies discussed above, which suggested that cofilin1 primarily contributed to LTP-induced spine enlargement by its F-actin severing activity (Bosch et al., 2014) and that cofilin1′s F-actin severing activity did not require CAP1 (Kotila et al., 2019). During LTP, the ratio of cofilin1 to actin transiently increased in dendritic spines (Bosch et al., 2014). At a high cofilin1-actin ratio, F-actin becomes saturated with cofilin1, and cofilin1-decorated filaments are stabilized in their 'twisted form' and can be used to nucleate filaments' growth (Bamburg and Bernstein, 2010). This could be an alternate explanation for a CAP1-independent function of cofilin1 in spine enlargement during LTP. Apart from CAP1, mammals express a second family member, namely CAP2, which is abundant in striated muscles and brain (Rust and Marcello, 2022). While analyses in systemic mutant mice revealed important functions for CAP2 in heart physiology and skeletal muscle development (Peche et al., 2012; Field et al., 2015; Kepser et al., 2019; Xiong et al., 2019), its function in the brain largely remained unknown. A recent study revealed that LTP triggered the interaction of CAP2 with cofilin1 in hippocampal neurons, which was required for postsynaptic cofilin1 translocation, spine remodeling and synaptic potentiation (Pelucchi et al., 2020b). Hence, CAP2 appeared to be more relevant than CAP1 for structural plasticity during LTP.

While CAP1 seems to only play a minor role in structural plasticity associated with cLTP, our data revealed that it is more relevant for structural changes associated with cLTD induced at physiological temperature. Specifically, we found increased myc-CAP1 concentration in dendritic spines upon cLTD induction, which was especially pronounced in thin spines. While cLTD induced a decrease in the density of thin and mushroom-like spines in CTR neurons, it only slightly decreased thin spine density, but not mushroom-like spine density in CAP1-KO neurons. Different from LTP, a precise time course of cofilin1 activity during LTD has not been investigated in single spines to date. However, a crucial role for cofilin1 in LTD-induced structural plasticity has been described almost twenty years ago (Zhou et al., 2004; Morishita et al., 2005), and subsequent studies identified signaling molecules including the phosphatases calcineurin and slingshot that promote cofilin1 activation during LTD or the scaffolding protein β-arrestin-2 that controls postsynaptic recruitment of cofilin1 during LTD (Zhou et al., 2004; Wang et al., 2005; Pontrello et al., 2012). Collectively, these studies led to the model that cofilin1 is required for F-actin disassembly and, hence, for spine shrinkage during LTD (Rust, 2015a; Ben Zablah et al., 2020). Interestingly, a low frequency stimulation protocol, which reportedly reduced synaptic transmission and triggered spine shrinkage (Zhou et al., 2004; Görlich et al., 2011; Görlich et al., 2012), failed in inducing LTD in hippocampal CA3-CA1 synapses from cofilin1-KO mice, but instead caused a slight increase in synaptic transmission (Rust et al., 2010). Based on this finding and the increased average spine size upon cLTD induction in CAP1-KO neurons, it is quite conceivable that CAP1 and cofilin1 cooperate in F-actin disassembly and spine shrinkage during LTD.

In conclusion, we here reported that induction of cLTP and cLTD oppositely altered myc-CAP1 concentration in dendritic spines, with cLTP decreasing and cLTD increasing it (Fig. 6A). Further, we showed that cLTP-induced structural plasticity was only mildly affected by CAP1 inactivation, while cLTD failed in inducing spine shrinkage in CAP1-KO neurons, but instead slightly increased average spine size presumably due to a reduction in the number of small spines (Fig. 6B). From our data we concluded that CAP1 is more relevant for cLTD, while a previous study linked the family member CAP2 to structural changes associated with LTP (Pelucchi et al., 2020b).

CRediT authorship contribution statement

Experiments were performed by AH, experiments were designed and results were discussed by AH and MBR, manuscript was written by MBR and AH.

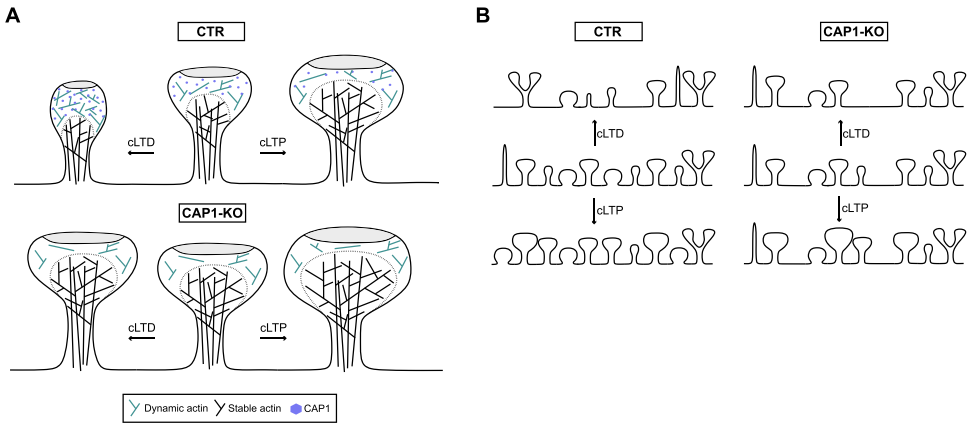

Fig. 6. Proposed model of CAP1's role in synaptic plasticity. (A) CAP1 is important for spine shrinkage. Spine head concentration of CAP1 increases during cLTD to promote actin depolymerization and spine size reduction. CAP1 spine head concentration decreases during cLTP to decelerate actin depolymerization and facilitate spine stabilization. Loss of CAP1 leads to an enlargement of the stable actin pool and an increase in spine size. During cLTD, CAP1-deficient neurons fail to induce spine shrinkage in large, stable spines. cLTP further enhances spine enlargement in CAP1-KO neurons. **(B)** cLTP leads to spine enlargement and a more mature spine profile in CTR neurons. In CAP1-KO neurons, cLTP only induces further spine size increase of large spines, but no alterations in spine type distribution. cLTD induces retraction and shrinkage of dendritic spines in CTR neurons. CAP1-KO neurons fail to shrink large, stable spines and are only moderately able to retract smaller, less stable spines.

Declaration of Competing Interest

The authors declare that they have no known competing financial interests or personal relationships that could have appeared to influence the work reported in this paper.

Acknowledgments

The authors thank Eva Becker, Flynn Kubeja and Renate Gondrum for excellent technical support. This work was supported by research grants from Fondazione Cariplo (2018-0511) and from Deutsche Forschungsgemeinschaft (DFG, German Research Foundation) RU 1232/10-1 to MBR. Open access funding provided by the Open Access Publishing Fund of Philipps-Universität Marburg with support of the DFG.

Appendix A. Supporting information

Supplementary data associated with this article can be found in the online version at doi:10.1016/j.ejcb.2023.151357.

References

Bamburg, J.R., Bernstein, B.W., 2010. Roles of ADF/cofilin in actin polymerization and beyond. F1000 Biol. Rep. 2, 62.
Bamburg, J.R., Minamide, L.S., Wiggan, O., Tahtamouni, L.H., Kuhn, T.B., 2021. Cofilin and actin dynamics: multiple modes of regulation and their impacts in neuronal development and degeneration. Cells 10, 2726.
Ben Zablah, Y., Merovitch, N., Jia, Z., 2020. The role of ADF/cofilin in synaptic physiology and Alzheimer's disease. Front Cell Dev. Biol. 8, 594998.
Borovac, J., Bosch, M., Okamoto, K., 2018. Regulation of actin dynamics during structural plasticity of dendritic spines: signaling messengers and actin-binding proteins. Mol. Cell Neurosci. 91, 122–130.
Bosch, M., Hayashi, Y., 2012. Structural plasticity of dendritic spines. Curr. Opin. Neurobiol. 22, 383–388.
Bosch, M., Castro, J., Saneyoshi, T., Matsuno, H., Sur, M., Hayashi, Y., 2014. Structural and molecular remodeling of dendritic spine substructures during long-term potentiation. Neuron 82, 444–459.
Bourgeron, T., 2015. From the genetic architecture to synaptic plasticity in autism spectrum disorder. Nat. Rev. Neurosci. 16, 551–563.
Chaudhry, F., Breitsprecher, D., Little, K., Sharov, G., Sokolova, O., Goode, B.L., 2013. Srv2/cyclase-associated protein forms hexameric shurikens that directly catalyze actin filament severing by cofilin. Mol. Biol. Cell 24, 31–41.
Chen, J.H., Kellner, Y., Zagrebelsky, M., Grundwald, M., Korte, M., Walla, P.J., 2015. Two-photon correlation spectroscopy in single dendritic spines reveals fast actin filament reorganization during activity-dependent growth. PLoS One 10, e0128241.
Citri, A., Malenka, R.C., 2008. Synaptic plasticity: multiple forms, functions, and mechanisms. Neuropsychopharmacology 33, 18–41.
Duffney, L.J., Zhong, P., Wei, J., et al., 2015. Autism-like deficits in shank3-deficient mice are rescued by targeting actin regulators. Cell Rep. 11, 1400–1413.
Feuge, J., Scharkowski, F., Michaelsen-Preusse, K., Korte, M., 2019. FMRP modulates activity-dependent spine plasticity by binding Cofilin1 mRNA and regulating localization and local translation. Cereb. Cortex 29, 5204–5216.
Field, J., Ye, D.Z., Shinde, M., et al., 2015. CAP2 in cardiac conduction, sudden cardiac death and eye development. Sci. Rep. 5, 17256.
Goodson, M., Rust, M.B., Witke, W., Bannerman, D., Mott, R., Ponting, C.P., Flint, J., 2012. Cofilin-1: a modulator of anxiety in mice. PLoS Genet 8, e1002970.
Görlich, A., Wolf, M., Zimmermann, A.M., Gurniak, C.B., Al Banchaabouchi, M., Sassoe-Pognetto, M., Witke, W., Friauf, E., Rust, M.B., 2011. N-Cofilin can compensate for the loss of ADF in excitatory synapses. PLoS One 6, e26789.
Görlich, A., Zimmermann, A.M., Schober, D., Bottcher, R.T., Sassoe-Pognetto, M., Friauf, E., Witke, W., Rust, M.B., 2012. Preserved morphology and physiology of excitatory synapses in profilin1-deficient mice. PLoS One 7, e30068.
Gu, J., Lee, C.W., Fan, Y., et al., 2010. ADF/cofilin-mediated actin dynamics regulate AMPA receptor trafficking during synaptic plasticity. Nat. Neurosci. 13, 1208–1215.
Heinze, A., Schuldt, C., Khudayberdiev, S., et al., 2022. Functional interdependence of the actin regulators CAP1 and cofilin1 in control of dendritic spine morphology. Cell Mol. Life Sci. 79, 558.
Hering, H., Sheng, M., 2001. Dendritic spines: structure, dynamics and regulation. Nat. Rev. Neurosci. 2, 880–888.
Hotulainen, P., Llano, O., Smirnov, S., Tanhuanpaa, K., Faix, J., Rivera, C., Lappalainen, P., 2009. Defining mechanisms of actin polymerization and depolymerization during dendritic spine morphogenesis. J. Cell Biol. 185, 323–339.
Ichetovkin, I., Grant, W., Condeelis, J., 2002. Cofilin produces newly polymerized actin filaments that are preferred for dendritic nucleation by the Arp2/3 complex. Curr. Biol. 12, 79–84.
Jansen, S., Collins, A., Golden, L., Sokolova, O., Goode, B.L., 2014. Structure and mechanism of mouse cyclase-associated protein (CAP1) in regulating actin dynamics. J. Biol. Chem. 289, 30732–30742.
Kandel, E.R., Dudai, Y., Mayford, M.R., 2014. The molecular and systems biology of memory. Cell 157, 163–186.
Kepser, L.J., Damar, F., De Cicco, T., Chaponnier, C., Proszynski, T.J., Pagenstecher, A., Rust, M.B., 2019. CAP2 deficiency delays myofibril actin cytoskeleton differentiation and disturbs skeletal muscle architecture and function. Proc. Natl. Acad. Sci. USA 116, 8397–8402.
Kotila, T., Kogan, K., Enkavi, G., Guo, S., Vattulainen, I., Goode, B.L., Lappalainen, P., 2018. Structural basis of actin monomer re-charging by cyclase-associated protein. Nat. Commun. 9, 1892.
Kotila, T., Wioland, H., Enkavi, G., Kogan, K., Vattulainen, I., Jegou, A., Romet-Lemonne, G., Lappalainen, P., 2019. Mechanism of synergistic actin filament pointed end depolymerization by cyclase-associated protein and cofilin. Nat. Commun. 10, 5320.
Morishita, W., Marie, H., Malenka, R.C., 2005. Distinct triggering and expression mechanisms underlie LTD of AMPA and NMDA synaptic responses. Nat. Neurosci. 8, 1043–1050.
Normoyle, K.P., Brieher, W.M., 2012. Cyclase-associated protein (CAP) acts directly on F-actin to accelerate cofilin-mediated actin severing across the range of physiological pH. J. Biol. Chem. 287, 35722–35732.
Okabe, S., 2020. Regulation of actin dynamics in dendritic spines: Nanostructure, molecular mobility, and signaling mechanisms. Mol. Cell Neurosci. 109, 103564.
Okamoto, K., Nagai, T., Miyawaki, A., Hayashi, Y., 2004. Rapid and persistent modulation of actin dynamics regulates postsynaptic reorganization underlying bidirectional plasticity. Nat. Neurosci. 7, 1104–1112.
Oser, M., Condeelis, J., 2009. The cofilin activity cycle in lamellipodia and invadopodia. J. Cell Biochem 108, 1252–1262.
Ouyang, Y., Wong, M., Capani, F., et al., 2005. Transient decrease in F-actin may be necessary for translocation of proteins into dendritic spines. Eur. J. Neurosci. 22, 2995–3005.
Peche, V.S., Holak, T.A., Burgute, B.D., et al., 2012. Ablation of cyclase-associated protein 2 (CAP2) leads to cardiomyopathy. Cell Mol. Life Sci. 70, 527–543.
Pelucchi, S., Stringhi, R., Marcello, E., 2020a. Dendritic spines in Alzheimer's disease: how the actin cytoskeleton contributes to synaptic failure. Int. J. Mol. Sci. **21**.

Pelucchi, S., Vandermeulen, L., Pizzamiglio, L., et al., 2020b. Cyclase-associated protein 2 dimerization regulates cofilin in synaptic plasticity and Alzheimer's disease. Brain Commun. 2, fcaa086.
Pinzon-Parra, C.A., Coatl-Cuaya, H., Diaz, A., Guevara, J., Rodriguez-Moreno, A., Flores, G., 2022. Long-term effect of neonatal antagonism of ionotropic glutamate receptors on dendritic spines and cognitive function in rats. J. Chem. Neuroanat. 119, 102054.
Pontrello, C.G., Sun, M.Y., Lin, A., Fiacco, T.A., DeFea, K.A., Ethell, I.M., 2012. Cofilin under control of beta-arrestin-2 in NMDA-dependent dendritic spine plasticity, long-term depression (LTD), and learning. Proc. Natl. Acad. Sci. USA 109, E442–E451.
Rocha, M., Sur, M., 1995. Rapid acquisition of dendritic spines by visual thalamic neurons after blockade of N-methyl-D-aspartate receptors. Proc. Natl. Acad. Sci. USA 92, 8026–8030.
Rust, M.B., 2015a. ADF/cofilin: a crucial regulator of synapse physiology and behavior. Cell Mol. Life Sci. 72, 3521–3529.
Rust, M.B., 2015b. Novel functions for ADF/cofilin in excitatory synapses - lessons from gene-targeted mice. Commun. Integr. Biol. 8, e1114194.
Rust, M.B., Marcello, E., 2022. Disease association of cyclase-associated protein (CAP): lessons from gene-targeted mice and human genetic studies. Eur. J. Cell Biol. 101, 151207.
Rust, M.B., Maritzen, T., 2015c. Relevance of presynaptic actin dynamics for synapse function and mouse behavior. Exp. Cell Res. 335, 165–171.
Rust, M.B., Gurniak, C.B., Renner, M., et al., 2010. Learning, AMPA receptor mobility and synaptic plasticity depend on n-cofilin-mediated actin dynamics. EMBO J. 29, 1889–1902.
Rust, M.B., Khudayberdiev, S., Pelucchi, S., Marcello, E., 2020. CAPt'n of actin dynamics: recent advances in the molecular, developmental and physiological functions of cyclase-associated protein (CAP). Front. Cell Dev. Biol. 8, 586631.
Schneider, F., Duong, T.A., Metz, I., Winkelmeier, J., Hubner, C.A., Endesfelder, U., Rust, M.B., 2021a. Mutual functional dependence of cyclase-associated protein 1 (CAP1) and cofilin1 in neuronal actin dynamics and growth cone function. Prog. Neurobiol. 202, 102050.
Schneider, F., Metz, I., Khudayberdiev, S., Rust, M.B., 2021b. Functional redundancy of cyclase-associated proteins CAP1 and CAP2 in differentiating neurons. Cells 10, 1525.
Schratt, G.M., Tuebing, F., Nigh, E.A., Kane, C.G., Sabatini, M.E., Kiebler, M., Greenberg, M.E., 2006. A brain-specific microRNA regulates dendritic spine development. Nature 439, 283–289.
Shankar, G.M., Li, S., Mehta, T.H., et al., 2008. Amyloid-beta protein dimers isolated directly from Alzheimer's brains impair synaptic plasticity and memory. Nat. Med 14, 837–842.
Shekhar, S., Chung, J., Kondev, J., Gelles, J., Goode, B.L., 2019. Synergy between Cyclase-associated protein and Cofilin accelerates actin filament depolymerization by two orders of magnitude. Nat. Commun. 10, 5319.
Shinoda, Y., Tanaka, T., Tominaga-Yoshino, K., Ogura, A., 2010. Persistent synapse loss induced by repetitive LTD in developing rat hippocampal neurons. PLoS One 5, e10390.
Spence, E.F., Soderling, S.H., 2015. Actin out: regulation of the synaptic cytoskeleton. J. Biol. Chem. 290, 28613–28622.
Sungur, A.O., Stemmler, L., Wohr, M., Rust, M.B., 2018. Impaired object recognition but normal social behavior and ultrasonic communication in cofilin1 mutant mice. Front Behav. Neurosci. 12, 25.
Tada, T., Sheng, M., 2006. Molecular mechanisms of dendritic spine morphogenesis. Curr. Opin. Neurobiol. 16, 95–101.
Wang, Y., Shibasaki, F., Mizuno, K., 2005. Calcium signal-induced cofilin dephosphorylation is mediated by Slingshot via calcineurin. J. Biol. Chem. 280, 12683–12689.
Wolf, M., Zimmermann, A.M., Gorlich, A., Gurniak, C.B., Sassoe-Pognetto, M., Friauf, E., Witke, W., Rust, M.B., 2015. ADF/Cofilin controls synaptic actin dynamics and regulates synaptic vesicle mobilization and exocytosis. Cereb. Cortex 25, 2863–2875.
Xiong, Y., Bedi, K., Berritt, S., Attipoe, B.K., Brooks, T.G., Wang, K., Margulies, K.B., Field, J., 2019. Targeting MRTF/SRF in CAP2-dependent dilated cardiomyopathy delays disease onset. JCI Insight 4, e124629.
Yang, Y., Liu, J.J., 2022. Structural LTP: signal transduction, actin cytoskeleton reorganization, and membrane remodeling of dendritic spines. Curr. Opin. Neurobiol. 74, 102534.
Zhang, Z., Ye, M., Li, Q., et al., 2019. The schizophrenia susceptibility gene OPCML regulates spine maturation and cognitive behaviors through Eph-cofilin signaling. Cell Rep. 29, 49–61 e47.
Zhou, Q., Homma, K.J., Poo, M.M., 2004. Shrinkage of dendritic spines associated with long-term depression of hippocampal synapses. Neuron 44, 749–757.
Zimmermann, A.M., Jene, T., Wolf, M., Gorlich, A., Gurniak, C.B., Sassoe-Pognetto, M., Witke, W., Friauf, E., Rust, M.B., 2015. Attention-deficit/hyperactivity disorder-like phenotype in a mouse model with impaired actin dynamics. Biol. Psychiatry 78, 95–106.